Vitamin D Receptor in Osteoblasts Is a Negative Regulator of Bone Mass Control

Yoko Yamamoto, Tatsuya Yoshizawa, Toru Fukuda, Yuko Shirode-Fukuda, Taiyong Yu, Keisuke Sekine, Takashi Sato, Hirotaka Kawano, Ken-ichi Aihara, Yuko Nakamichi, Tomoyuki Watanabe, Masayo Shindo, Kazuki Inoue, Erina Inoue, Naoya Tsuji, Maiko Hoshino, Gerard Karsenty, Daniel Metzger, Pierre Chambon, Shigeaki Kato, and Yuuki Imai

Institute of Molecular and Cellular Biosciences (Y.Y., T.Yo., T.F., Y.S-F., T.Yu, K.S., T.S., H.K., K.A., Y.N., T.W., M.S., K.I., E.I., N.T., M.H., Y.I.), The University of Tokyo, Bunkyo-ku, 113-0032, Japan; Department of Genetics and Development (G.K.), Columbia University Medical Center, New York, New York; Institut de Génétique et de Biologie Moléculaire et Cellulaire (D.M., P.C.), Centre National de la Recherche Scientifique, Institut National de la Santé et de la Recherche Médicale, Université Louis Pasteur, Collège de France, 67404 Illkirch, Strasbourg, France; and Soma Central Hospital (S.K.), Fukushima, Japan.

The physiological and beneficial actions of vitamin D in bone health have been experimentally and clinically proven in mammals. The active form of vitamin D [1α,25(OH)$_2$D$_3$] binds and activates its specific nuclear receptor, the vitamin D receptor (VDR). Activated VDR prevents the release of calcium from its storage in bone to serum by stimulating intestinal calcium absorption and renal reabsorption. However, the direct action of VDR in bone tissue is poorly understood because serum Ca^{2+} homeostasis is maintained through tightly regulated ion transport by the kidney, intestine, and bone. In addition, conventional genetic approaches using *VDR* knockout (VDR-KO, *VDR*$^{-/-}$) mice could not identify VDR action in bone because of the animals' systemic defects in calcium metabolism. In this study, we report that systemic *VDR* heterozygous KO (*VDR*$^{+/L-}$) mice generated with the Cre/loxP system as well as conventional *VDR* heterozygotes (*VDR*$^{+/-}$) showed increased bone mass in radiological assessments. Because mineral metabolism parameters were unaltered in both types of mice, these bone phenotypes imply that skeletal VDR plays a role in bone mass regulation. To confirm this assumption, osteoblast-specific VDR-KO (*VDR*$^{\Delta Ob/\Delta Ob}$) mice were generated with 2.3 kb α1(I)-collagen promoter-*Cre* transgenic mice. They showed a bone mass increase without any dysregulation of mineral metabolism. Although bone formation parameters were not affected in bone histomorphometry, bone resorption was obviously reduced in *VDR*$^{\Delta Ob/\Delta Ob}$ mice because of decreased expression of receptor activator of nuclear factor kappa-B ligand (an essential molecule in osteoclastogenesis) in *VDR*$^{\Delta Ob/\Delta Ob}$ osteoblasts. These findings establish that VDR in osteoblasts is a negative regulator of bone mass control. **(*Endocrinology* 154: 1008–1020, 2013)**

Vitamin D acting through its steroid hormone, 1α,25(OH)$_2$D$_3$, exerts a wide variety of biological actions in many target organs. Studies have firmly established the pivotal roles of 1α,25(OH)$_2$D$_3$ in calcium homeostasis, mineral metabolism, associated bone formation, and metabolism (1–3). Thus, it is well accepted that 1α,25(OH)$_2$D$_3$ is a positive factor for bone development and maintaining bone mineral density (BMD) (4). Such beneficial action of 1α,25(OH)$_2$D$_3$ for bone health is supported by clinical treatment with vitamin D and the clinical success achieved with vitamin D analogues as antiosteoporotic agents (5–7). Moreover, its impact in the cytodifferentiation of certain precursor cell types has been demonstrated (8, 9). These biological actions of 1α,25(OH)$_2$D$_3$ are believed to be mediated primarily through the nuclear vitamin D receptor (VDR). VDR is a

ISSN Print 0013-7227 ISSN Online 1945-7170
Printed in U.S.A.

doi: 10.1210/en.2012-1542 Received May 16, 2012. Accepted December 28, 2012.
First Published Online February 6, 2013

Abbreviations: BMD, bone mineral density; ES, embryonic stem; FBS, fetal bovine serum; RANKL, receptor activator of nuclear factor kappa-B ligand; SXA, single-energy X-ray absorptiometry; TRAP, tartrate-resistant acid phosphatase; VDR, vitamin D receptor; VDR-KO, VDR knockout.

member of the nuclear hormone receptor gene family and serves as a ligand-dependent transcription factor to transcriptionally control expression of a set of target genes (10–12).

The expected significance of VDR in the biological actions of $1\alpha,25(OH)_2D_3$ has been verified by analyses of human mutations and genetically engineered mouse models. Rachitic abnormalities observed in patients with type II hereditary rickets could be recapitulated by ablation of the *Vdr* gene in mice (conventional *Vdr* knockout [VDR-KO] mice) (13, 14). Interestingly, rachitic abnormalities in patients and mutant mice looked similar to those induced by nutritional vitamin D deficiency except for alopecia. However, $1\alpha,25(OH)_2D_3$ supplements were not effective at ameliorating rachitic abnormalities. Moreover, impaired bone formation or growth in *Vdr* mutants could not be rescued by $1\alpha,25(OH)_2D_3$ (15). However, feeding normal diets with a reduced phosphate content and high mineral content improved bone growth or formation in conventional VDR-KO mice (16, 17). Those findings implied that the positive effects of $1\alpha,25(OH)_2D_3$ in bone development and mineral deposition are mediated by indirect actions, such as increases in serum mineral levels.

The concept that $1\alpha,25(OH)_2D_3$ might have indirect beneficial actions in bone homeostasis in intact animals has been hampered by in vitro findings. In contrast to its beneficial actions in vivo, $1\alpha,25(OH)_2D_3$ induces receptor activator of nuclear factor kappa-B ligand (RANKL), a major osteoclastogenic factor, in vitro (18–20). Thus, the action of $1\alpha,25(OH)_2D_3$ on the skeleton has been enigmatic because of the contrast between in vivo and in vitro findings. In skeletal tissue, the direct action of $1\alpha,25(OH)_2D_3$ in vivo is poorly understood for several reasons. First, activated VDR prevents calcium release from bone to serum through its stimulation of intestinal calcium absorption and renal reabsorption. Second, serum Ca^{2+} homeostasis is maintained as a result of tightly regulated ion transport by the kidney, intestine, and bone. Finally, conventional genetic approaches using VDR-KO ($VDR^{-/-}$) mice could not identify VDR action in bone because of the animals' systemic defect in calcium metabolism.

We established previously a genetic approach using the Cre-loxP system (21) to selectively ablate *Vdr* to accurately assess VDR function in a given tissue or cell type. During our characterization of *Vdr* floxed mice (*Vdr* ablated in the whole body, designated as systemic VDR-KO [$VDR^{L-/L-}$] mice), we found that systemic heterozygous VDR-KO ($VDR^{+/L-}$) mice exhibited increased bone mass without endocrine mineral metabolism being affected. This bone phenotype was also seen in heterozygous mutant mice in which *Vdr* was ablated by a conventional approach ($VDR^{+/-}$). Furthermore, osteoblast-specific VDR-KO mice ($VDR^{\Delta Ob/\Delta Ob}$) exhibited similar increases in bone mass and mineral density with decreased bone resorption. Together with the data from in vitro coculture assays of osteoblasts and osteoclasts, the current findings demonstrate that VDR in extraskeletal tissues is a positive regulator of bone mass control, whereas skeletal VDR serves as an attenuator of bone growth and remodeling.

Materials and Methods

Generation of systemic and osteoblast-specific VDR-KO mice

A genomic DNA fragment of *Vdr* was isolated from a TT2 embryonic stem (ES) cell (22) genomic library by using a rat *Vdr* cDNA as a probe. The targeting vector was created by inserting a single *loxP* site and the *tk-neo* cassette with two *loxP* sites into the SphI site and the BamHI site, respectively. Targeted TT2 ES cells, identified by Southern blot analysis, were electroporated with the *Cre* expression vector to excise the *tk-neo* cassette and obtain the VDR^{L2} targeted clones. The targeted TT2 ES clones, identified by Southern blot analysis, were aggregated with single eight-cell embryos from CD-1 mice to generate chimeras, as described previously (14, 23). Floxed *VDR* mice ($VDR^{L2/+}$), originally in a hybrid C57BL/6 and CBA genetic background, were backcrossed into a C57BL/6J background. Floxed *VDR* mice were crossed with *CMV-Cre* transgenic mice [$CMV\text{-}Cre^{(tg/0)}$, C57BL/6J background] (24) to generate $CMV\text{-}Cre^{(tg/0)}/VDR^{L-/+}$ and then crossed with C57BL/6J wild-type mice to remove the *CMV-Cre* transgene. $VDR^{L-/+}$ mice were crossed to generate systemic VDR-KO mice ($VDR^{L-/L-}$). Mouse a1(I)-collagen promoter-*Cre* transgenic mice [$Col1a1\text{-}Cre^{(tg/0)}$] (25), originally on a FVB genetic background, were backcrossed into a C57BL/6J background. $VDR^{L2/+}$ mice were crossed with $Col1a1\text{-}Cre^{(tg/0)}$ mice to generate $Col1a1\text{-}Cre^{(tg/0)}/VDR^{L2/+}$. Osteoblast-specific VDR-KO mice ($VDR^{\Delta Ob/\Delta Ob}$, $Col1a1\text{-}Cre^{(tg/0)}/VDR^{L2/L2}$) were obtained by crossing $Col1a1\text{-}Cre^{(tg/0)}/VDR^{L2/+}$ male mice with $VDR^{L2/+}$ female mice. Offspring were genotyped either by Southern blotting or by PCR using a specific pair of primers. The following sets of primers were used: WT (491 bp) and L2 (575 bp), 5′-CAACCTTGGTGAGCTGAGTTTAC-3′ and 5′-CACAGCAGGAGTGGGATTACTGATATT-3′; L- (338 bp), 5′-AAAGACACTGGCTGCCAACC-3′ and 5′-TGACAGTGCCCTGTTCTTCC-3′. *Cre* transgenes (507 bp) were detected by PCR using a specific pair of primers, 5′-TTCCCGCAGAACCTGAAGATGTTCGCG-3′ and 5′-CATCAGCTACACCAGAGACGGAAATCC-3′. All mice were housed in a specific-pathogen-free facility under climate-controlled conditions with a 12 h light/dark cycle and were provided with water and standard diet (CE-2, CLEA Japan, Tokyo, Japan) or high calcium diet (CE-2 supplemented with 2% calcium, 1.25% phosphate and 20% lactose, CLEA Japan) ad libitum. All animals were maintained according to the protocol approved by the Animal Care and Use Committee of the University of Tokyo.

Serum biochemistry

Serum levels of calcium, phosphate, PTH, and $1,25(OH)_2D$ were measured at a commercial laboratory (SRL, Tokyo, Japan). Serum FGF23 levels were determined using FGF-23 ELISA Kit (Kainos Laboratories, Tokyo, Japan).

Analysis of skeletal morphology

Bone radiographs of femora were taken with a soft X-ray apparatus (TRS-1005, SOFRON, Tokyo, Japan). BMD was measured by single-energy X-ray absorptiometry (SXA) using a bone mineral analyzer (DCS-600EX-III; ALOKA, Tokyo, Japan). Bone histomorphometric measurements of osteoblast-specific VDR-KO mice were performed at a commercial laboratory (Kureha Special Laboratory, Fukushima, Japan). In brief, an intraperitoneal injection of calcein (1.6 mg/kg body weight) was administrated for in vivo fluorescent labeling twice at an interval of 72 h. Mice were killed at 48 h after the second injection. Tibiae were fixed in 70% ethanol and embedded in methyl methacrylate without decalcification. Bone sections were prepared and subjected to bone histomorphometry. Histomorphometry of the secondary spongiosa was performed with a semiautomated system for bone analysis (Histometry RT Camera, System Supply, Nagano, Japan) at 400-fold magnification. Nomenclature, symbols, and units are those recommended by the Nomenclature Committee of the American Society for Bone and Mineral Research (26). Histomorphometry of the proximal tibial metaphyses of systemic VDR-KO mice were performed for four optical fields of the proximal border immediately adjacent to the growth plate using the OsteoMeasure histomorphometry system (OsteoMetrics, Decatur, Georgia) at 200-fold magnification. Microcomputed tomographic (μCT) analysis of femora was performed using a Scanco Medical μCT35 System (Scanco Medical, Brüttisellen, Switzerland) with an isotropic voxel size of 6 μm (high-resolution) for trabecular analyses and 12 μm (medium resolution) for cortical analyses according to the manufacturer's instructions and the recent guidelines of the American Society for Bone and Mineral Research (27). Scans were conducted in 70% ethanol and used an X-ray tube potential of 70 kVp, an X-ray intensity of 0.114 mA, and an integration time of 400 ms. From the scans of the distal femur, a region beginning proximal to the growth plate and extending 1.73 to 2.76 mm proximally and a region of 2.4 mm in length and the center at the midpoint of the femur was selected for quantitative volumetric analyses of metaphyseal trabecular and diaphyseal cortical microstructures, respectively. The image slices were reconstructed using Scanco μCT Version 6.1 software (Scanco Medical). For tartrate-resistant acid phosphatase (TRAP) staining, lumbar vertebrae were fixed in 4% paraformaldehyde overnight and dehydrated with graded ethanol and embedded in methyl methacrylate without decalcification. Bone sections (4 μm thick) were prepared with a microtome (Leica RM2255, Leica Microsystems, Wetzlar, Germany) and subjected to TRAP staining followed by counterstaining with hematoxylin.

Real-time RT-PCR

Total RNA was extracted with TRIzol (Invitrogen, Life Technologies, Carlsbad, California) and subsequently treated with DNase I (TAKARA BIO INC, Otsu, Japan). First-strand cDNA was synthesized from total RNA using PrimeScript RT Master Mix (TAKARA BIO INC) and subjected to real-time RT-PCR using SYBR Premix Ex Taq II (TAKARA BIO INC) or KAPA SYBR Fast qPCR Kits (KAPA Biosystems, Boston, Massachusetts) with Thermal Cycler Dice (TAKARA BIO INC) according to the manufacturer's instructions. Primers were purchased from TAKARA BIO INC or Operon Biotechnologies (Tokyo, Japan) (23).

Cell culture

Primary osteoblasts were isolated from calvariae of 2-day-old mice according to a method reported previously (28). Calvariae were cut into small pieces and embedded in a type I collagen gel (Cellmatrix Type I-A, Nitta Gelatin Inc, Osaka, Japan). After 4 days of culture, osteoblasts grown from the calvariae were isolated by digestion of collagen gels with collagenase (Wako, Osaka, Japan) and suspended in αMEM containing 10% fetal bovine serum (FBS) and cultured until confluent. Primary osteoblasts were then differentiated in αMEM containing 10% FBS, 50 μg/mL ascorbic acid, and 10 mM β-glycerophosphate for 7 days or cocultured with bone marrow macrophages in αMEM containing 10% FBS supplemented with 10^{-8} M $1\alpha,25(OH)_2D_3$ (Cayman Chemical, Ann Arbor, Michigan) for 7 days.

Isolation of the osteocyte fraction

Osteocytes were isolated from calvariae as reported previously (29) with modification. Briefly, calvariae were dissected from 12-day-old mice and subjected to six sequential, 30-minute digestions in PBS containing 0.05% trypsin, 0.53 mM EDTA, and 1.5 U/mL collagenase-P (Roche Applied Science, Mannheim, Germany) at 37°C. Cell fractions four to six were collected and suspended in high glucose DMEM containing 10% FBS. Cells were centrifuged and resuspended in TRIzol for RNA extraction.

Statistical analysis

Data were analyzed by two-tailed Student t test. For all graphs, data are represented as means ± SD. Statistical significance was accepted at $P < .05$.

Results

VDR$^{L-/L-}$ mice exhibited typical features of vitamin D-dependent type II rickets

To precisely assess VDR's function in target organs, a Cre-loxP system was applied to generate floxed *VDR* mice by introducing *loxP* sites in the *VDR* gene locus (Figure 1). The floxed mutation was genetically transmitted, and floxed *VDR* mice were born at Mendelian frequencies. No obvious morphological abnormalities were seen even in aged floxed mice. To examine whether the expected excision of DNA between two *loxP* sites by Cre recombinase was inducible in vivo, floxed *VDR* mice were crossed with *Cre* transgenic mice [*CMV-Cre*$^{(tg/0)}$] driven by a universal CMV promoter (24) to generate *CMV-Cre*$^{(tg/0)}$/*VDR*$^{L-/+}$ offspring that were then crossed with C57BL/6J wild-type mice to remove the *CMV-Cre* transgene. Resultant

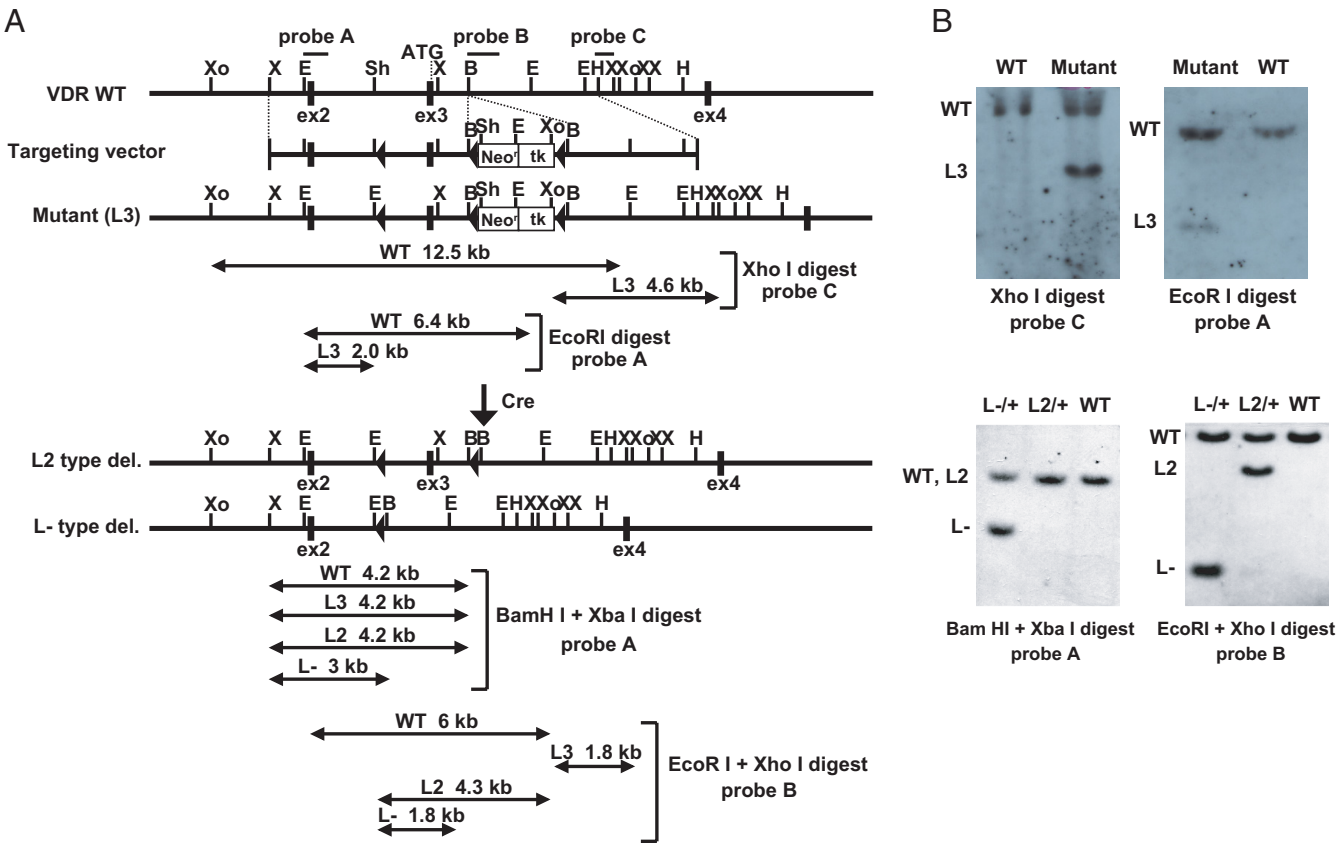

Figure 1. Generation of floxed *VDR* ($VDR^{L2/+}$) mice. A, Illustration of the targeting strategy. Black boxes and arrowheads represent exons and *loxP* sites, respectively. Abbreviations: B, BamHI; E, EcoRI; Sh, SphI; X, XbaI; Xo, XhoI. B, Southern blot analyses of embryonic stem (ES) cells. Genomic DNA isolated from ES cells electroporated with the targeting vector (upper) and from targeted ES cells electroporated with the *Cre* expression vector (lower) were digested with the indicated restriction enzymes and hybridized with the indicated probes.

$VDR^{L-/+}$ mice were further crossed to obtain systemic VDR-KO mice ($VDR^{L-/L-}$).

To confirm ablation of the *Vdr* gene using this approach, $VDR^{L-/L-}$ mice were compared with conventional VDR-KO mice ($VDR^{-/-}$) in regard to the expected rachitic abnormalities (14). Conventional VDR-KO mice exhibited typical features of vitamin D-dependent type II rickets, such as growth retardation, hypocalcemia, secondary hyperparathyroidism, impaired bone formation, and alopecia (13, 14). Most of conventional VDR-KO mice died within 15 weeks of birth (14). Similar observations were made in $VDR^{L-/L-}$ mice, including growth retardation (Figure 2A), alopecia (Figure 2B), hypocalcemia, hypophosphatemia, secondary hyperparathyroidism, and elevated serum levels of $1,25(OH)_2D$ (Figure 2C). $VDR^{L-/L-}$ mice fed a normal calcium diet were generally debilitated with weight loss after 9 weeks and died within 15 weeks of birth. High-calcium diets prevented lethality in $VDR^{L-/L-}$ mice and $VDR^{-/-}$ mice (data not shown). Soft X-ray images (Figure 2D) and μCT analysis (Figure 2, E and F) of femora showed impaired bone formation. Villanueva-Goldner staining (Figure 2G) and histomorphometric analysis on primary spongiosa (Figure 2H) of proximal tibial metaphyses showed disorganized growth plate morphology, as well as a significant increase in osteoid volume. These observations confirmed complete *Vdr* ablation in $VDR^{L-/L-}$ mice, the same as observed in $VDR^{-/-}$ mice (14).

$VDR^{+/L-}$ as well as $VDR^{+/-}$ mice showed increased bone mass without overt rachitic abnormalities

During our detailed characterization of $VDR^{L-/L-}$ mice, we found that systemic *VDR* heterozygous KO ($VDR^{+/L-}$) mice exhibited increased bone mass at the age of 18 weeks (Figure 3, D-G). No rachitic features such as growth retardation (Figure 2A), alopecia (Figure 3A), hypocalcemia, hypophosphatemia, or elevated serum levels of $1,25(OH)_2D$ (Figure 3B) were obvious in $VDR^{+/L-}$ mice. Villanueva-Goldner staining of proximal tibial metaphyses (Figure 3C) and soft X-ray images of femora (Figure 3D) showed normal bone mineralization and morphology, respectively. BMD analyzed by SXA (Figure 3E) showed increased bone mass in $VDR^{+/L-}$ mice. μCT analysis (Figure 3, F and G) also showed increased trabecular bone volume of the distal femoral metaphyses of $VDR^{+/L-}$ mice. Because conventional VDR-KO heterozy-

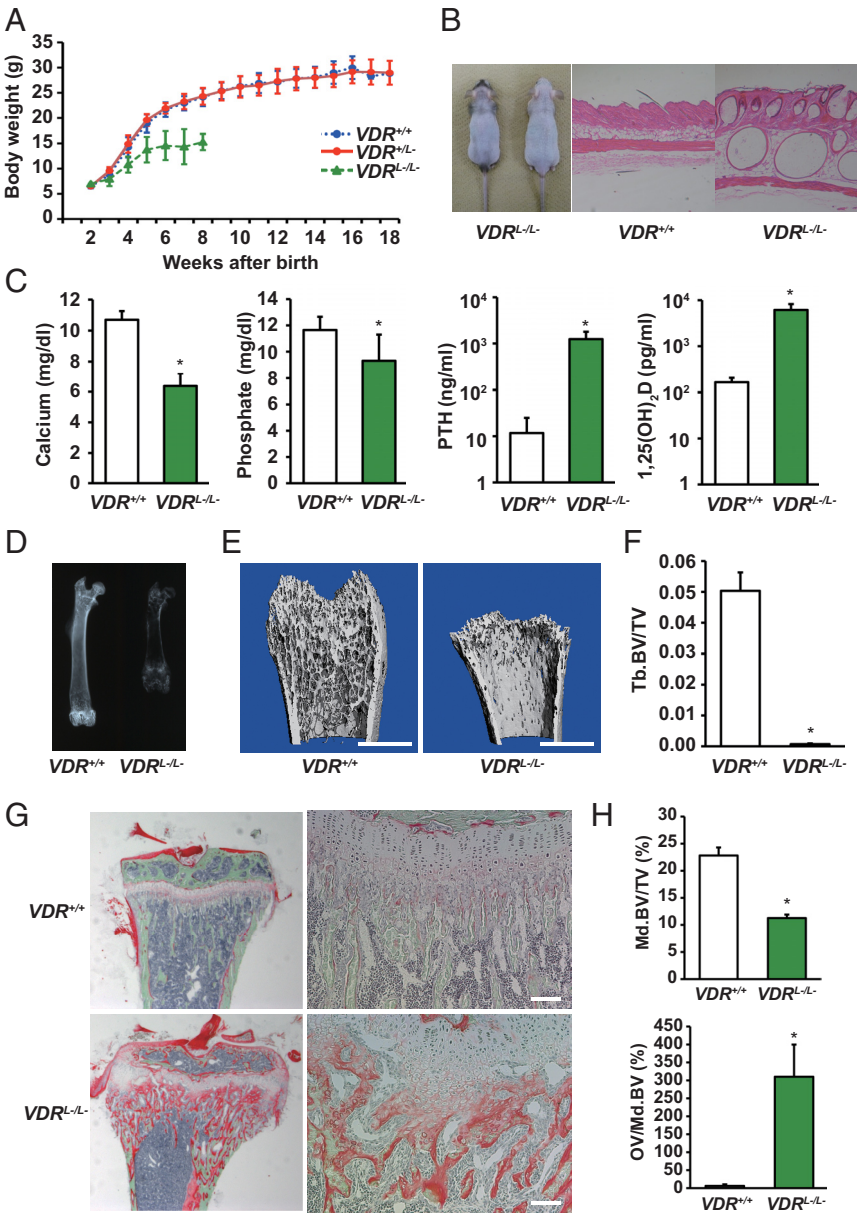

Figure 2. $VDR^{L-/L-}$ mice exhibited features typical of vitamin D-dependent type II rickets. A, Growth curves of mice. n ≥ 4 for each genotype. The line of $VDR^{L-/L-}$ was terminated at 8 weeks because $VDR^{L-/L-}$ mice were generally debilitated with weight loss after 9 weeks and died within 15 weeks after birth. B, Appearance of 27- (left) and 41-week-old (right) $VDR^{L-/L-}$ mice and hematoxylin and eosin staining of skin sections of 26-week-old mice fed a high-calcium diet. C, Biochemical analysis of 6-week-old mice. n ≥ 4 for each genotype. *$P < .05$ compared with $VDR^{+/+}$ mice. D, Soft X-ray images of femora in 6-week-old mice. E, Three-dimensional microcomputed tomographic (μCT) images of distal femora in 6-week-old mice. Scale bar: 1 mm. F, Quantitative μCT analysis of trabecular structure on 460 microtomographic slices (2.76 mm) at the distal femur in 6-week-old mice. n = 5 for each genotype. *$P < .05$ compared with $VDR^{+/+}$ mice. G, Villanueva-Goldner staining of proximal tibiae in 6-week-old mice. Lower (left) and higher (right) magnification images of growth plate and cancellous bone are indicated. Mineralized bone and unmineralized osteoid are stained green and red, respectively. Scale bar: 100 μm. H, Histomorphometric analysis on primary spongiosa of proximal tibial metaphyses performed at proximal border immediately adjacent to the growth plate in 6-week-old mice. Abbreviations: Md.BV/TV, mineralized bone volume per tissue volume; OV/Md.BV, osteoid volume per mineralized bone volume. n = 3 for each genotype. *$P < .05$ compared with $VDR^{+/+}$ mice.

gous male mice generated by other methods (13) had normal skeletal development until 16 weeks of age (30), we re-examined the bone phenotype in conventional *VDR* heterozygous KO mice ($VDR^{+/-}$) generated by our group (14). As reported previously (14), no rachitic features such as growth retardation (Figure 3, H and I) or alopecia (Figure 3H) were obvious in $VDR^{+/-}$ mice. Although soft X-ray images of femora (Figure 3J) showed normal bone morphology, even in $VDR^{+/-}$ mice at the age of 16 weeks, BMD data were higher than those of their wild-type littermates (Figure 3K). μCT analysis (Figure 3, L and M) also showed increased trabecular bone volume of the distal femoral metaphyses of $VDR^{+/-}$ mice. Because mineral metabolism parameters and endocrine markers were unaltered in both heterozygotes, these bone phenotypes imply that skeletal VDR plays a role in bone mass regulation.

Selective ablation of *Vdr* in osteoblasts in mice with normal mineral metabolism

To directly assess the function of VDR in bone, *Vdr* was selectively ablated in osteoblasts by crossing the floxed *VDR* mice with a1(I)-collagen promoter-*Cre* transgenic mice [$Col1a1\text{-}Cre^{(tg/0)}$] driven by an osteoblast-specific 2.3 kb mouse a1(I)-collagen promoter (25). The *loxP* excision in osteoblasts was confirmed by X-gal staining of the whole embryo and bone sections of mice generated by crossing $Col1a1\text{-}Cre^{(tg/0)}$ mice with tester mice carrying an *lacZ* transgene (25). Osteoblast-selective *Cre* recombination in $Col1a1\text{-}Cre^{(tg/0)}/VDR^{L2/L2}$ mice was tested by Southern blot analysis of gDNA prepared from various tissues from these mice. As shown in Figure 4A, DNA excision was seen exclusively in calvaria and long bones,

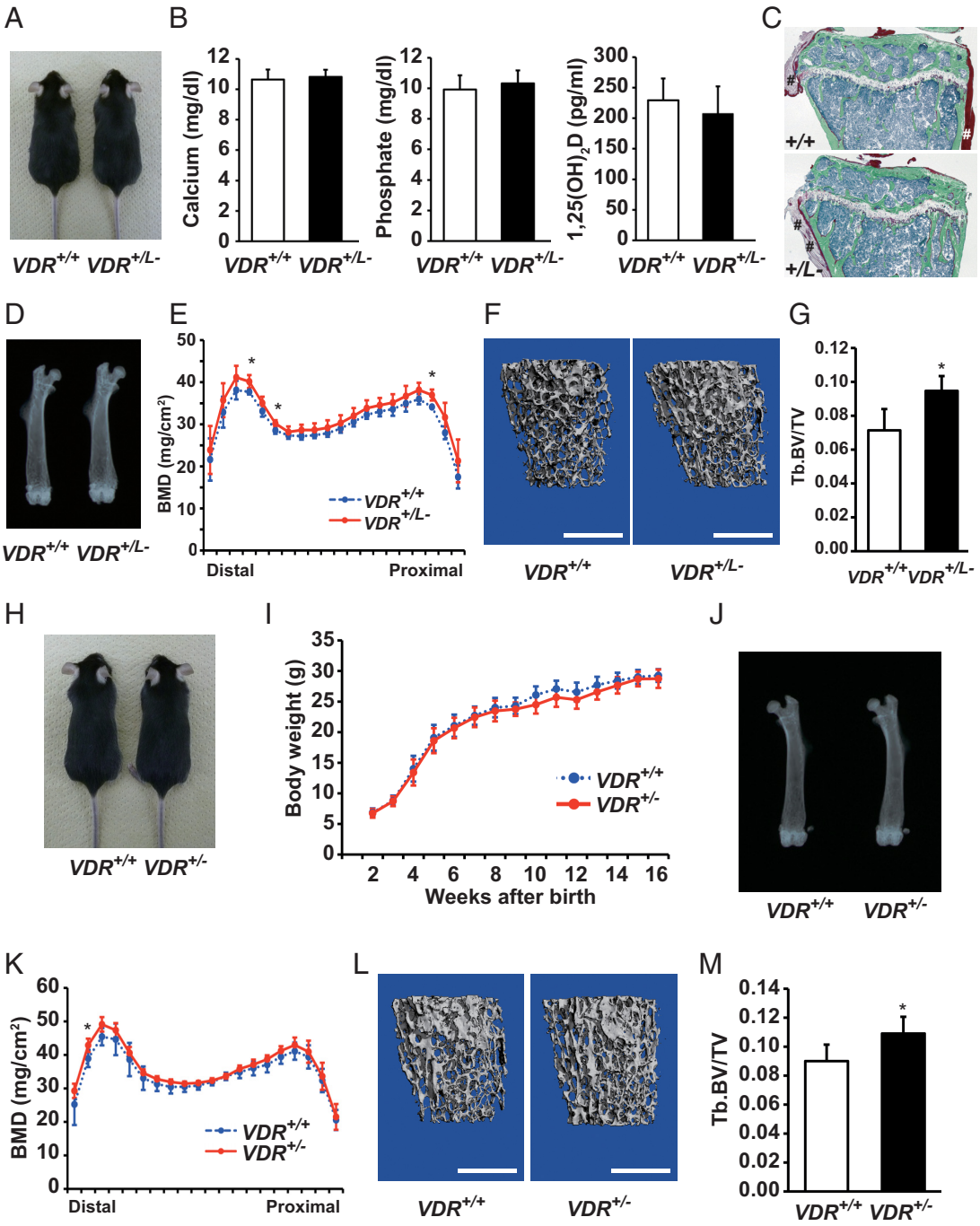

Figure 3. $VDR^{+/L-}$ as well as VDR^{+-} mice exhibited increased bone mass. A, Appearance of 18-week-old $VDR^{+/+}$ and $VDR^{+/L-}$ mice. B, Biochemical analysis of 18-week-old mice. n ≥ 4 for each genotype. C, Villanueva-Goldner staining of proximal tibial metaphyses in 18-week-old mice. #Indicates connective tissues. D, Soft X-ray images of femora in 18-week-old mice. Body weight-matched male littermates were analyzed. E, Bone mineral density (BMD) of each of 20 equal longitudinal divisions of femora from 18-week-old mice. Body weight-matched male littermates were analyzed. n = 4 for each genotype. *$P < .05$ compared with $VDR^{+/+}$ mice. F and G, Three-dimensional microcomputed tomographic (μCT) images of trabecular bone (F) and quantitative analysis of trabecular bone volume (G) on 400 microtomographic slices (2.4 mm) at the distal femoral metaphyses in 18-week-old mice. Body weight-matched male littermates were analyzed. Scale bar: 1 mm. n ≥ 4 for each genotype. *$P < .05$ compared with $VDR^{+/+}$ mice. H, Appearance of 9-week-old $VDR^{+/+}$ and $VDR^{+/-}$ mice. I, Growth curves of mice. n ≥ 5 for each genotype. J, Soft X-ray images of femora in 16-week-old mice. Body weight-matched male littermates were analyzed. K, BMD of each of 20 equal longitudinal divisions of femora from 16-week-old mice. Body weight-matched male littermates were analyzed. n ≥ 4 for each genotype. *$P < .05$ compared with $VDR^{+/+}$ mice. L and M, Three-dimensional μCT images of trabecular bone (L) and quantitative analysis of trabecular bone volume (M) on 400 microtomographic slices (2.4 mm) at the distal femoral metaphyses in 16-week-old mice. Body weight-matched male littermates were analyzed. Scale bar: 1 mm. n ≥ 6 for each genotype. *$P < .05$ compared with $VDR^{+/+}$ mice.

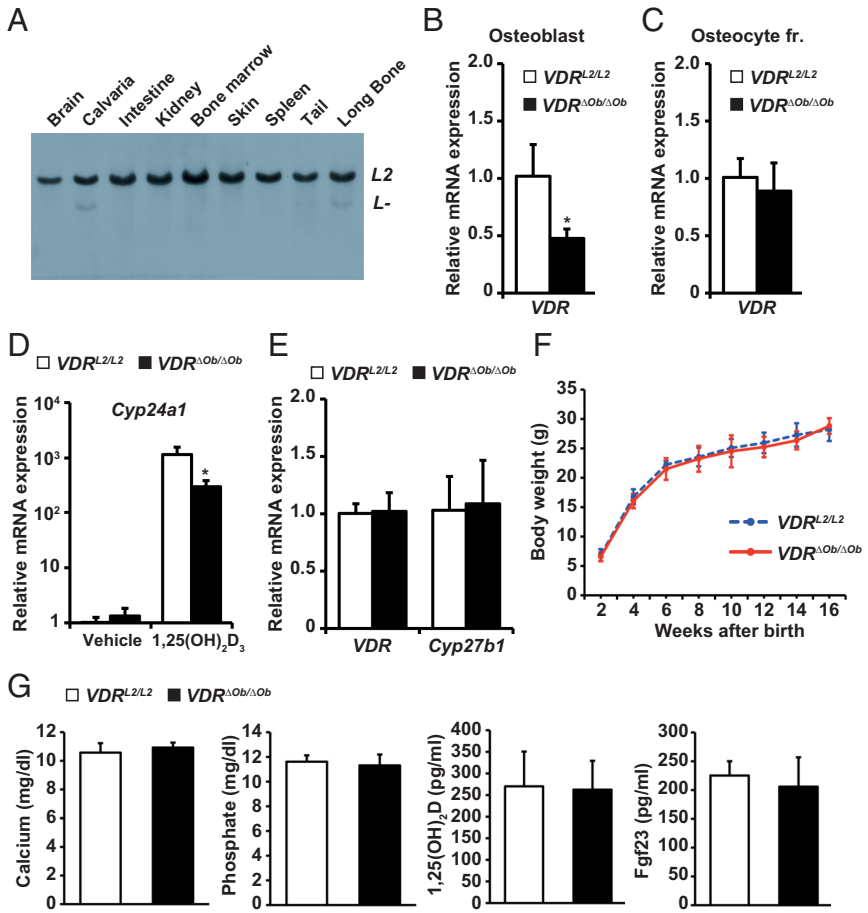

Figure 4. Normocalcemia and normophosphatemia in $VDR^{\Delta Ob/\Delta Ob}$ mice. A, Southern blot analysis of gDNA prepared from the indicated tissues of *VDRΔOb/ΔOb* mice. Genomic DNA was digested with BamHI and XbaI and hybridized with probe A in Figure 1A. B and C, *Vdr* gene expression in primary osteoblasts prepared from calvariae of newborn mice (B) and in an osteocyte-rich fraction prepared by sequential enzymatic digestion of calvariae of 12-day-old mice (C). Expression was assessed by real-time RT-PCR and normalized to that of *Gapdh*. n ≥ 3 for each genotype. Data are means ± SD of duplicate wells. $*P < .05$ compared with $VDR^{L2/L2}$ mice. D, Gene expression of *Cyp24a1* in primary osteoblasts prepared from calvariae of newborn mice treated with vehicle or $1\alpha,25(OH)_2D_3$ (10^{-8} M). Expression was assessed by real-time RT-PCR and normalized to that of *Gapdh*. n = 3 for each genotype. Data are means ± SD of duplicate wells. $*P < .05$ compared with $VDR^{L2/L2}$ mice. E, Gene expression of *VDR* and *Cyp27b1* in kidneys of 16-week-old mice. Expression was assessed by real-time RT-PCR and normalized to that of *Gapdh*. n = 4 for each genotype. Data are means ± SD of duplicate wells. F, Growth curves of mice. n ≥ 5 for each genotype. G, Biochemical analysis of 16-week-old mice. n ≥ 6 for each genotype.

whereas no obvious excision was detected in other tissues, including kidney and intestine, where VDR is a significant regulator of mineral metabolism. The level of *Vdr* mRNA expression was reduced in primary osteoblasts prepared from calvariae of newborn $Col1a1\text{-}Cre^{(tg/0)}/VDR^{L2/L2}$ mice when assessed by real-time RT-PCR (Figure 4B). However, no obvious reduction of *Vdr* mRNA expression was observed in an osteocyte-rich fraction prepared by sequential enzymatic digestion of calvariae of 12-day-old mice (Figure 4C). Partial VDR inactivation was confirmed by assessing $1\alpha,25(OH)_2D_3$-induced *Cyp24a1* mRNA expression in primary osteoblasts from $Col1a1\text{-}Cre^{(tg/0)}/VDR^{L2/L2}$ mice (Figure 4D). On the other hand, *VDR* and *Cyp27b1* mRNA expression in the kidneys of $Col1a1\text{-}Cre^{(tg/0)}/VDR^{L2/L2}$ mice was not altered (Figure 4E). Taken together, we conclude that the *Vdr* gene is selectively ablated in osteoblasts in $Col1a1\text{-}Cre^{(tg/0)}/VDR^{L2/L2}$ mice, hereafter designated as osteoblast-specific VDR-KO ($VDR^{\Delta Ob/\Delta Ob}$).

$VDR^{\Delta Ob/\Delta Ob}$ mice exhibited no obvious abnormalities in growth (Figure 4F) or in serum levels of calcium, phosphate, $1\alpha,25(OH)_2D$, or Fgf23 (Figure 4G). From the absence of overt rachitic abnormalities, we conclude that VDR in the extraskeletal tissues of $VDR^{\Delta Ob/\Delta Ob}$ mice was functionally normal.

Increased bone mass in $VDR^{\Delta Ob/\Delta Ob}$ mice

Although it was recently reported that the mice selectively deleted VDR in osteocyte/osteoblast using *Dmp1-Cre* showed no dysregulated phenotype in bone at 8 weeks of age (31). Although soft X-ray images of femora showed normal bone morphology (Figure 5A), BMD analyzed by SXA (Figure 5B) showed increased bone mass in $VDR^{\Delta Ob/\Delta Ob}$ mice when compared with their body weight-matched control littermates ($VDR^{L2/L2}$) at 16 weeks of age. μCT analysis (Figure 5, C and D) showed increased trabecular bone volume of the distal femoral metaphyses of $VDR^{\Delta Ob/\Delta Ob}$ mice at 16 weeks of age. However, no significant differences was observed in cortical thickness of the femoral midshaft of $VDR^{\Delta Ob/\Delta Ob}$ mice at 16 weeks of age (Figure 5, C and D) or in trabecular bone volume of the distal femoral metaphyses at 4 (Figure 5, E and F) or 9 weeks (Figure 5, G and H) of age.

Apparent increased bone mass with decreased bone resorption in $VDR^{\Delta Ob/\Delta Ob}$ mice

Histomorphometric analyses on secondary spongiosa of the proximal tibial metaphyses of 16-week-old mice revealed significant decreases in parameters of bone resorption, such as the numbers of osteoclasts and osteoclast

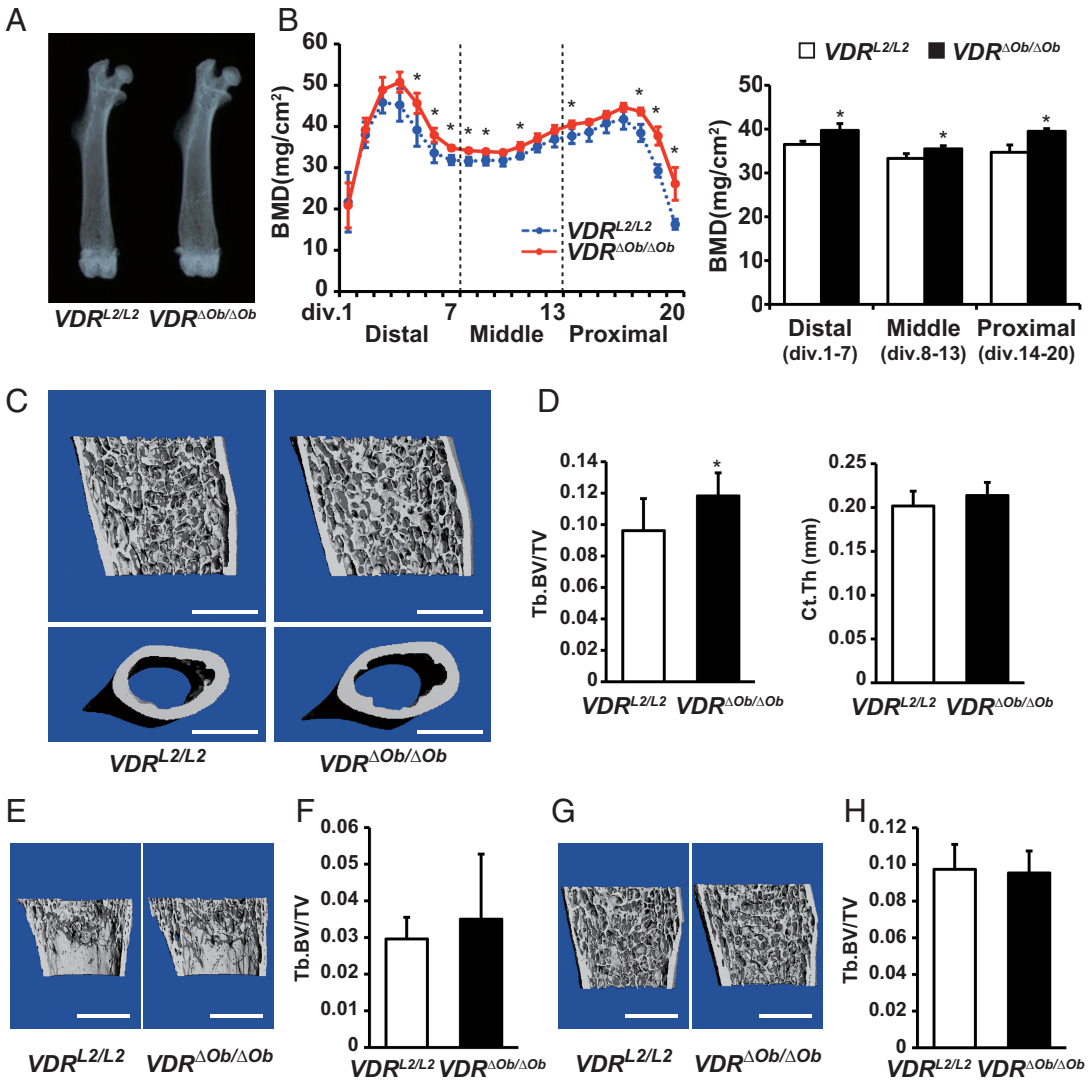

Figure 5. *VDR*$^{\Delta Ob/\Delta Ob}$ mice exhibit increased bone mass. A, Soft X-ray images of femora in 16-week-old mice. Body weight-matched male littermates were analyzed. B, Bone mineral density (BMD) of each of 20 equal longitudinal divisions (left) and of three regions (distal: division 1–7; middle: division 8–13; proximal: division 14–20, right) of femora from 16-week-old mice. Body weight-matched male littermates were analyzed. n = 4 for each genotype. *$P < .05$ compared with *VDR*$^{L2/L2}$ mice. C to H, Three-dimensional microcomputed tomographic (μCT) images (upper panels in C, E, G) and quantitative analysis of trabecular bone volume (D, F, H) on 400 (upper panels in C and D), and 288 (E and F), 376 (G and H) microtomographic slices (2.4, 1.73, 2.26 mm, respectively) at the distal femoral metaphyses and three-dimensional μCT images (lower panels in C) and quantitative analysis of cortical structure on 200 microtomographic slices (2.4 mm) at the femoral midshaft (D) in 16- (C and D), 4- (E and F), and 9-week-old mice (G and H). Body weight-matched male littermates were analyzed. Scale bar: 1 mm. n ≥ 6 (C and D) or n ≥ 4 (E-H) for each genotype. *$P < .05$ compared with *VDR*$^{L2/L2}$ mice.

surface in *VDR*$^{\Delta Ob/\Delta Ob}$ mice compared with those in *VDR*$^{L2/L2}$, whereas no statistically significant differences were found in parameters of bone formation, such as osteoblast surface, mineral apposition rate, bone formation rate, and mineralizing surface per bone surface (Figure 6A). TRAP staining of lumbar vertebrae in 16-week-old mice also showed decreased bone resorption in *VDR*$^{\Delta Ob/\Delta Ob}$ mice (Figure 6B).

Osteoblastic VDR-mediated vitamin D action in osteoclastogenesis through gene induction

To further assess the reasons of the increased bone mass caused by the decreased bone resorption in *VDR*$^{\Delta Ob/\Delta Ob}$ mice, we examined the expressions of marker genes associated with osteoblast/osteoclast development, as well as *Fgf23*. Among the tested markers in the tibia of *VDR*$^{\Delta Ob/\Delta Ob}$ mice (Figure 7A), a significant decrease was found in the mRNA level of *RANKL (Tnfsf11)*, which is a key factor for osteoclastogenesis expressed in osteoblasts (19, 32), chondrocytes (33, 34), and osteocytes (34, 35), as well as gene expressions of nuclear factor of activated T cells (*Nfatc1*), *c-fos*, and *Trap*. Although decreased expression of *Fgf23* in bone and reduced concentration of Fgf23 in the serum of chondrocyte-specific VDR-KO mice were reported (33), gene expression of *Fgf23* (Figure 7A) in bone and the concentration of Fgf23 in serum (Figure

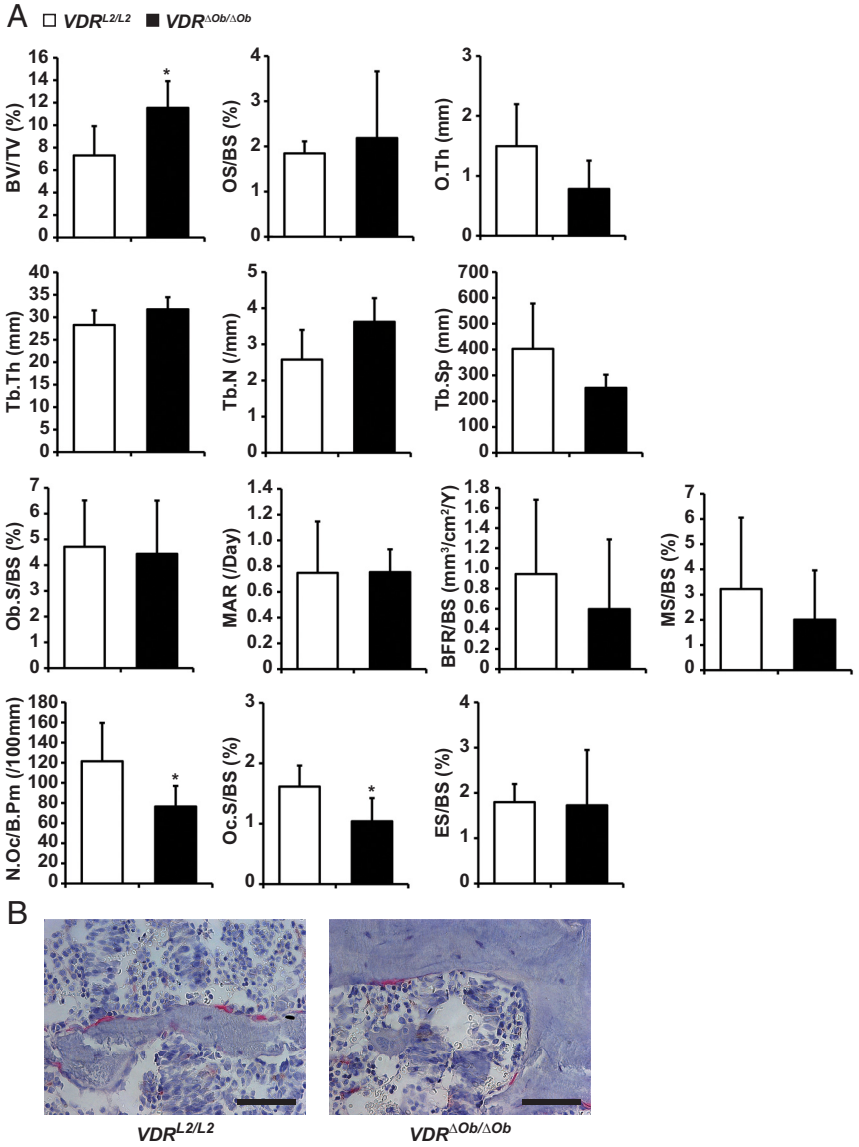

Figure 6. Increased bone mass with decreased bone resorption is apparent in $VDR^{\Delta Ob/\Delta Ob}$ mice. A, Bone histomorphometric analysis of proximal tibial metaphyses of 16-week-old mice. Abbreviations: BFR/BS, bone formation rate per bone surface; BV/TV, bone volume per tissue volume; ES/BS, eroded surface per bone surface; MAR, mineral apposition rate; MS/BS, mineralizing surface per bone surface; N. Oc/B.Pm, osteoclast number per bone perimeter; Ob.S/BS, osteoblast surface per bone surface; Oc.S/ BS, osteoclast surface per bone surface; OS/BS, osteoid surface per bone surface; O.Th, osteoid thickness; Tb.N, trabecular number; Tb.Sp, trabecular separation; Tb.Th, trabecular thickness. Body weight-matched male littermates were analyzed. n = 5 for each genotype. $*P < .05$ compared with $VDR^{L2/L2}$ mice. B, Tartrate-resistant acid phosphatase (TRAP) staining of lumbar sections of 16-week-old mice. Scale bar: 50 μm.

4G) were not altered in $VDR^{\Delta Ob/\Delta Ob}$ mice. Moreover, we examined gene expression of *RANKL* and *osteoprotegerin* (*Opg*, *Tnfrsf11b*, soluble decoy receptor of RANKL) in cultured osteoblasts. As shown in Figure 7B, the mRNA level of *RANKL* and the *RANKL/Opg* ratio, an index of osteoclastogenic stimulus, were significantly decreased in osteoblasts of $VDR^{\Delta Ob/\Delta Ob}$ mice treated with $1\alpha,25(OH)_2D_3$. On the other hand, the mRNA level of *RANKL* in the osteocyte fraction obtained from $VDR^{\Delta Ob/\Delta Ob}$ mice was not altered (Figure 7C). Thus, the observed decrease in bone resorption in $VDR^{\Delta Ob/\Delta Ob}$ mice is attributable to lowered osteoclastogenesis caused by the reduced level of *RANKL* expression in osteoblasts. To verify this idea, we examined whether osteoblast and osteoclast precursor cells derived from calvaria and bone marrow of $VDR^{\Delta Ob/\Delta Ob}$ mice could differentiate in response to known inducers, such as ascorbic acid and β-glycerophosphate (osteoblasts) and macrophage-colony stimulating factor and RANKL (osteoclasts) (19, 36–38). In the presence of such inducers, both osteoblastogenesis (Figure 7D) and osteoclastogenesis (Figure 7E) appeared indistinguishable between cells derived from $VDR^{\Delta Ob/\Delta Ob}$ and $VDR^{L2/L2}$ mice.

We then tested the osteoblastic action of $1\alpha,25(OH)_2D_3$ in an osteoclastogenesis assay using a coculture system in the presence of $1\alpha,25(OH)_2D_3$, a known inducer of osteoclast differentiation (19, 36, 37). When osteoblast precursor cells derived from calvaria and osteoclast precursor cells from bone marrow of $VDR^{L2/L2}$ mice were cocultured with $1\alpha,25(OH)_2D_3$, TRAP-positive staining was detected in multinuclear osteoclasts. However, the osteoblast and osteoclast precursor cells from $VDR^{\Delta Ob/\Delta Ob}$ mice were partially impaired in the response to $1\alpha,25(OH)_2D_3$ in the induction of osteoclastogenesis (Figure 7F). These results suggest that osteoblastic VDR mediates the $1\alpha,25(OH)_2D_3$ action for osteoclastogenesis, presumably through induction of *RANKL* gene expression. Taken together, these results suggest that VDR in intact bone is a negative regulator of bone mass through its stimulation of bone resorption via potentiation of RANKL-induced osteoclastogenesis.

Discussion

$1\alpha,25(OH)_2D_3$ is one of the best established hormones for enhancing bone health. Nutritional and pharmacologic

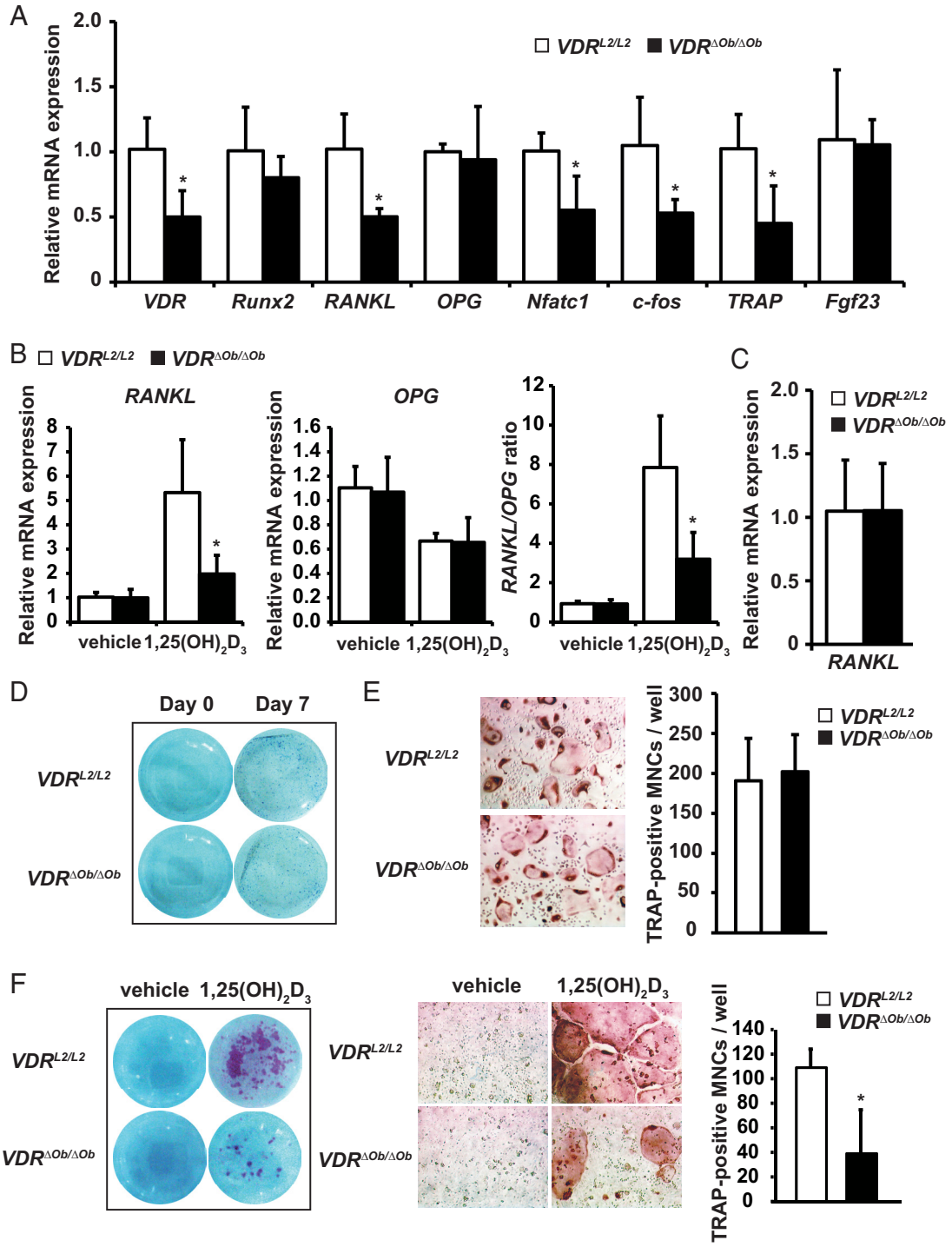

Figure 7. Osteoblastic VDR mediates $1,25(OH)_2D_3$ action in osteoclastogenesis through gene induction. A, Gene expression in tibiae of 16-week-old $VDR^{L2/L2}$ and $VDR^{\Delta Ob/\Delta Ob}$ mice. Expression was assessed by real-time RT-PCR and normalized to that of *Gapdh*. n = 3 for each genotype. Data are means ± SD of duplicate wells. $^*P < .05$ compared with $VDR^{L2/L2}$ mice. B, Gene expression of *RANKL* (left) and *Opg* (middle) and *RANKL/Opg* ratio (right) in primary osteoblasts prepared from calvariae of newborn mice treated with vehicle or $1\alpha,25(OH)_2D_3$ (10^{-8} M). Expression was assessed by real-time RT-PCR and normalized to that of *Gapdh*. n = 3 for each genotype. Data are means ± SD of duplicate wells. $^*P < .05$ compared with $VDR^{L2/L2}$ mice. C, *RANKL* gene expression in osteocyte-rich fractions prepared by sequential enzymatic digestion of calvariae of 12-day-old mice. Expression was assessed by real-time RT-PCR and normalized to that of *Gapdh*. n ≥ 3 for each genotype. Data are means ± SD of duplicate wells. D, ALP staining of primary osteoblasts differentiated by 50 μg/mL ascorbic acid and 10 mM β-glycerophosphate for 7 days. E, Osteoclast formation in vitro. Bone marrow macrophages were cultured in the presence of 20 ng/mL macrophage-colony stimulating factor and 100 ng/mL RANKL. After 4 days, the number of TRAP-positive multinucleated cells (MNCs) (left) per well was counted (right). n = 6 for each genotype. F, Primary osteoblasts and bone marrow macrophages were cocultured with $1\alpha,25(OH)_2D_3$ (10^{-8} M). After 7 days, cells were fixed and stained for TRAP (left). Magnified views of TRAP-positive cells in left panels are indicated (middle). The number of tartrate-resistant acid phosphatase (TRAP)-positive MNCs per well was counted (right). n = 3 for each genotype. $^*P < .05$ compared with $VDRL^{2/L2}$ mice.

treatments with natural and synthetic vitamin D-related compounds have successfully potentiated bone quality and mass (5–7). Nevertheless, the skeletal actions of $1\alpha,25(OH)_2D_3$ remain enigmatic because pioneering works showed that $1\alpha,25(OH)_2D_3$ stimulates bone resorption in a variety of in vitro culture systems of bone tissues and cells (19, 36–38). On the other hand, there are reports that $1\alpha,25(OH)_2D_3$ produces rapid biological responses that involve opening of chloride and calcium channels to activate exocytosis of bone matrix proteins such as osteocalcin (39, 40). However, because of a lack of experimental evidence in animals, it has not been verified that $1\alpha,25(OH)_2D_3$ acts directly on skeletal tissues as a negative effector. In the current study, we confirmed the in vitro findings in intact mice using genetic approaches to ablate VDR. The heterozygous VDR mutant mice ($VDR^{+/L-}$) ablated by the Cre-loxP system exhibited increased bone mass and BMD without any overt rachitic abnormalities (Figure 3). This bone phenotype previously was overlooked in our original description of conventional VDR-KO heterozygotes ($VDR^{+/-}$) and was attributed to individual differences related to insufficient backcrossing of genetic background.

Selective ablation of *Vdr* in osteoblasts resulted in increased bone mass and BMD in the absence of systemic defects in 16-week-old mice (Figure 5), although a recent study reported that late osteoblast/osteocyte-specific VDR knockout mice using *Dmp1-Cre* mice did not exhibit an abnormal bone phenotype at 8 weeks after birth (31). This inconsistency might be caused by the ages at which the animals were examined because $VDR^{\Delta Ob/\Delta Ob}$ mice also did not show a significant bone phenotype at 4 or 9 weeks after birth when compared with control littermates (Figure 5, E-H). These findings suggest that activated VDR in intact bone (presumably in osteoblasts) is a negative regulator of bone mass and mineral deposition in mature and nongrowing mice. On this point, there is a limitation in this study; we could not clarify different significance of VDR function in osteoblast between young and old mice. In addition, although these skeletal phenotypes have not yet been reported in humans, it would be interesting to assess bone phenotypes in humans bearing mutations in *VDR*, which presumably lead to partial dysfunction of VDR.

The function of skeletal VDR remains elusive since the current study uncovered the physiological impact of VDR in osteoblasts but not in osteoclasts. Furthermore, osteoblasts are functionally different, depending on the stages of cellular differentiation (41). The other transgenic mouse lines expressing *Cre* in osteoblasts of various differentiation stages will be useful to define osteoblastic VDR function when the mice are analyzed at maturity. From the current findings, RANKL appears to mediate, at least in part, the osteoblastic functions of activated VDR in osteoclastogenesis, although osteoblasts and other types of cells can produce RANKL and facilitate osteoclastogenesis (33–35). From this point of view, there is one possibility to explain why young $VDR^{\Delta Ob/\Delta Ob}$ mice did not exhibit increased bone mass, although osteoblasts prepared from neonatal calvariae of these mice impaired to express RANKL in response to $1\alpha,25(OH)_2D_3$. During maturation, there is the greatest osteoclastic bone resorption at primary spongiosa. At that time, most RANKL might be produced by chondrocytes in growth plate, rather than osteoblasts (33–35). In addition, it is conceivable that osteoclastic VDR plays a role in bone remodeling (42) based on the mutual interactions in function and cytodifferentiation between osteoblasts and osteoclasts (43–45). Nevertheless, the current findings force us to reconsider the bone phenotype observed in conventional *Vdr* null mutant mice (13, 14). The observed impairments in bone mass and remodeling are unlikely to be entirely attributed to the absence of VDR in the whole body, especially because of reduced calcium absorption from the intestine and secondary hyperparathyroidism. In this respect, to avoid systemic influences, as mentioned, mouse lines with selectively ablated *Vdr* in a specific type of bone cells will be useful for examining these ideas. From the current observations, the absence of *Vdr* might increase bone mass in vivo associated with reduction of *RANKL* gene expression. In addition, it was reported that overexpression of *Vdr* solely in mature osteoblasts driven by the human osteocalcin promoter led to increased bone mass because of inhibition of osteoclastogenesis associated with an altered OPG response and resulting imbalances in RANKL/OPG production (46). Increased bone mass caused by a deficiency at an early differentiation/maturation stage and an excess of *Vdr* in late stage osteoblasts indicates that an adequate protein level of VDR in osteoblasts might support maintenance of bone homeostasis via transcriptional regulation of each differentiation/maturation stage-specific target gene.

In summary, we present in vivo evidence that VDR in osteoblasts is a negative regulator of bone mass. Although $1\alpha,25(OH)_2D_3$ and its derivatives are commonly used as antiosteoporotic drugs, side effects, such as hypercalcemia and hypercalciuria, occasionally occur in such patients (47). Here, we show that osteoblast-specific ablation of VDR resulted in a bone mass increase without any dysregulation of mineral metabolism. Thus, we propose osteoblastic VDR, instead of $1\alpha,25(OH)_2D_3$ and its derivatives, as a novel therapeutic target for osteoporosis.

Acknowledgments

We thank Drs. Hisashi Murayama and Makoto Kajiwara (the hard tissue research team at Kureha Special Laboratory) for technical assistance; Drs. Makoto Makishima, Shigeyuki Uno, and Michiyasu Ishizawa (Division of Biochemistry, Department of Biomedical Sciences, Nihon University School of Medicine) for providing conventional VDR-KO mice on a C57BL/6 background; and Mai Yamaki and Haruko Higuchi for manuscript preparation.

Address all correspondence and requests for reprints to: Dr. Yuuki Imai, Institute of Molecular and Cellular Biosciences, The University of Tokyo, Bunkyo-ku, 113-0032, Japan. E-mail: yimai@iam.u-tokyo.ac.jp.

This work was supported by Grant-in-Aids from Japan Society for the Promotion of Science and the Ministry of Education, Culture, Sports, Science and Technology, Japan (to Y.Y., S.K., Y.I.).

Disclosure Summary: The authors have nothing to disclose.

References

1. **Walters MR.** Newly identified actions of the vitamin D endocrine system. *Endocr Rev*. 1992;13:719–764.
2. **Bouillon R, Okamura WH, Norman AW.** Structure-function relationships in the vitamin D endocrine system. *Endocr Rev*. 1995;16:200–257.
3. **DeLuca HF.** Evolution of our understanding of vitamin D. *Nutr Rev*. 2008;66:S73–87.
4. **Holick MF.** Vitamin D and bone health. *J Nutr*. 1996;126:1159S–1164S.
5. **Matsumoto T, Ito M, Hayashi Y, Hirota T, Tanigawara Y, Sone T, Fukunaga M, Shiraki M, Nakamura T.** A new active vitamin D3 analog, eldecalcitol, prevents the risk of osteoporotic fractures—a randomized, active comparator, double-blind study. *Bone*. 2011;49:605–612.
6. **Richy F, Schacht E, Bruyere O, Ethgen O, Gourlay M, Reginster JY.** Vitamin D analogs versus native vitamin D in preventing bone loss and osteoporosis-related fractures: a comparative meta-analysis. *Calcif Tissue Int*. 2005;76:176–186.
7. **Tilyard MW, Spears GF, Thomson J, Dovey S.** Treatment of postmenopausal osteoporosis with calcitriol or calcium. *N Engl J Med*. 1992;326:357–362.
8. **Mora JR, Iwata M, von Andrian UH.** Vitamin effects on the immune system: vitamins A and D take centre stage. *Nat Rev Immunol*. 2008;8:685–698.
9. **Samuel S, Sitrin MD.** Vitamin D's role in cell proliferation and differentiation. *Nutr Rev*. 2008;66:S116–124.
10. **Haussler MR, Whitfield GK, Haussler CA, Hsieh JC, Thompson PD, Selznick SH, Dominguez CE, Jurutka PW.** The nuclear vitamin D receptor: biological and molecular regulatory properties revealed. *J Bone Miner Res*. 1998;13:325–349.
11. **Kato S.** The function of vitamin D receptor in vitamin D action. *J Biochem*. 2000;127:717–722.
12. **Christakos S, Dhawan P, Liu Y, Peng X, Porta A.** New insights into the mechanisms of vitamin D action. *J Cell Biochem*. 2003;88:695–705.
13. **Li YC, Pirro AE, Amling M, Delling G, Baron R, Bronson R, Demay MB.** Targeted ablation of the vitamin D receptor: an animal model of vitamin D-dependent rickets type II with alopecia. *Proc Natl Acad Sci USA*. 1997;94:9831–9835.
14. **Yoshizawa T, Handa Y, Uematsu Y, Takeda S, Sekine K, Yoshihara Y, Kawakami T, Arioka K, Sato H, Uchiyama Y, Masushige S, Fukamizu A, Matsumoto T, Kato S.** Mice lacking the vitamin D receptor exhibit impaired bone formation, uterine hypoplasia and growth retardation after weaning. *Nat Genet*. 1997;16:391–396.
15. **Bouillon R, Carmeliet G, Verlinden L, van Etten E, Verstuyf A, Luderer HF, Lieben L, Mathieu C, Demay M.** Vitamin D and human health: lessons from vitamin D receptor null mice. *Endocr Rev*. 2008;29:726–776.
16. **Li YC, Amling M, Pirro AE, Priemel M, Meuse J, Baron R, Delling G, Demay MB.** Normalization of mineral ion homeostasis by dietary means prevents hyperparathyroidism, rickets, and osteomalacia, but not alopecia in vitamin D receptor-ablated mice. *Endocrinology*. 1998;139:4391–4396.
17. **Masuyama R, Nakaya Y, Katsumata S, Kajita Y, Uehara M, Tanaka S, Sakai A, Kato S, Nakamura T, Suzuki K.** Dietary calcium and phosphorus ratio regulates bone mineralization and turnover in vitamin D receptor knockout mice by affecting intestinal calcium and phosphorus absorption. *J Bone Miner Res*. 2003;18:1217–1226.
18. **Kitazawa R, Mori K, Yamaguchi A, Kondo T, Kitazawa S.** Modulation of mouse RANKL gene expression by Runx2 and vitamin D3. *J Cell Biochem*. 2008;105:1289–1297.
19. **Suda T, Takahashi N, Udagawa N, Jimi E, Gillespie MT, Martin TJ.** Modulation of osteoclast differentiation and function by the new members of the tumor necrosis factor receptor and ligand families. *Endocr Rev*. 1999;20:345–357.
20. **Pike JW.** Genome-wide principles of gene regulation by the vitamin D receptor and its activating ligand. *Mol Cell Endocrinol*. 2011;347:3–10.
21. **Li M, Indra AK, Warot X, Brocard J, Messaddeq N, Kato S, Metzger D, Chambon P.** Skin abnormalities generated by temporally controlled RXRalpha mutations in mouse epidermis. *Nature*. 2000;407:633–636.
22. **Yagi T, Tokunaga T, Furuta Y, Nada S, Yoshida M, Tsukada T, Saga Y, Takeda N, Ikawa Y, Aizawa S.** A novel ES cell line, *TT2, with high germline-differentiating potency*. *Anal Biochem*. 1993;214:70–76.
23. **Nakamura T, Imai Y, Matsumoto T, Sato S, Takeuchi K, Igarashi K, Harada Y, Azuma Y, Krust A, Yamamoto Y, Nishina H, Takeda S, Takayanagi H, Metzger D, Kanno J, Takaoka K, Martin TJ, Chambon P, Kato S.** Estrogen prevents bone loss via estrogen receptor alpha and induction of Fas ligand in osteoclasts. *Cell*. 2007;130:811–823.
24. **Dupé V, Davenne M, Brocard J, Dollé P, Mark M, Dierich A, Chambon P, Rijli FM.** In vivo functional analysis of the = Hoxa-1 3′ retinoic acid response element (3′RARE). *Development*. 1997;124:399–410.
25. **Dacquin R, Starbuck M, Schinke T, Karsenty G.** Mouse alpha1(I)-collagen promoter is the best known promoter to drive efficient Cre recombinase expression in osteoblast. *Dev Dyn*. 2002;224:245–251.
26. **Parfitt AM, Drezner MK, Glorieux FH, Kanis JA, Malluche H, Meunier PJ, Ott SM, Recker RR.** Bone histomorphometry: standardization of nomenclature, symbols, and units. Report of the ASBMR Histomorphometry Nomenclature Committee. *J Bone Miner Res*. 1987;2:595–610.
27. **Bouxsein ML, Boyd SK, Christiansen BA, Guldberg RE, Jepsen KJ, Müller R.** Guidelines for assessment of bone microstructure in rodents using micro-computed tomography. *J Bone Miner Res*. 2010;25:1468–1486.
28. **Takahashi N, Udagawa N, Akatsu T, Tanaka H, Isogai Y, Suda T.** Deficiency of osteoclasts in osteopetrotic mice is due to a defect in the local microenvironment provided by osteoblastic cells. *Endocrinology*. 1991;128:1792–1796.
29. **Paic F, Igwe JC, Nori R, Kronenberg MS, Franceschetti T, Harrington P, Kuo L, Shin DG, Rowe DW, Harris SE, Kalajzic I.** Iden-

tification of differentially expressed genes between osteoblasts and osteocytes. *Bone*. 2009;45:682–692.
30. **de Paula FJ, Dick-de-Paula I, Bornstein S, Rostama B, Le P, Lotinun S, Baron R, Rosen CJ.** VDR haploinsufficiency impacts body composition and skeletal acquisition in a gender-specific manner. *Calcif Tissue Int*. 2011;89:179–191.
31. **Lieben L, Masuyama R, Torrekens S, Van Looveren R, Schrooten J, Baatsen P, Lafage-Proust MH, Dresselaers T, Feng JQ, Bonewald LF, Meyer MB, Pike JW, Bouillon R, Carmeliet G.** Normocalcemia is maintained in mice under conditions of calcium malabsorption by vitamin D-induced inhibition of bone mineralization. *J Clin Invest*. 2012;122:1803–1815.
32. **Takayanagi H.** Osteoimmunology: shared mechanisms and crosstalk between the immune and bone systems. *Nat Rev Immunol*. 2007;7:292–304.
33. **Masuyama R, Stockmans I, Torrekens S, Van Looveren R, Maes C, Carmeliet P, Bouillon R, Carmeliet G.** Vitamin D receptor in chondrocytes promotes osteoclastogenesis and regulates FGF23 production in osteoblasts. *J Clin Invest*. 2006;116:3150–3159.
34. **Xiong J, Onal M, Jilka RL, Weinstein RS, Manolagas SC, O'Brien CA.** Matrix-embedded cells control osteoclast formation. *Nat Med*. 2011;17:1235–1241.
35. **Nakashima T, Hayashi M, Fukunaga T, Kurata K, Oh-Hora M, Feng JQ, Bonewald LF, Kodama T, Wutz A, Wagner EF, Penninger JM, Takayanagi H.** Evidence for osteocyte regulation of bone homeostasis through RANKL expression. *Nat Med*. 2011;17:1231–1234.
36. **Aubin JE, Bonnelye E.** Osteoprotegerin and its ligand: a new paradigm for regulation of osteoclastogenesis and bone resorption. *Osteoporos Int*. 2000;11:905–913.
37. **Takahashi N, Yamana H, Yoshiki S, Roodman GD, Mundy GR, Jones SJ, Boyde A, Suda T.** Osteoclast-like cell formation and its regulation by osteotropic hormones in mouse bone marrow cultures. *Endocrinology*. 1988;122:1373–1382.
38. **Teitelbaum SL, Ross FP.** Genetic regulation of osteoclast development and function. *Nat Rev Genet*. 2003;4:638–649.
39. **Mizwicki MT, Keidel D, Bula CM, Bishop JE, Zanello LP, Wurtz JM, Moras D, Norman AW.** Identification of an alternative ligand-binding pocket in the nuclear vitamin D receptor and its functional importance in 1alpha,25(OH)2-vitamin D3 signaling. *Proc Natl Acad Sci U S A*. 2004;101:12876–12881.
40. **Zanello LP, Norman AW.** Rapid modulation of osteoblast ion channel responses by 1alpha,25(OH)2-vitamin D3 requires the presence of a functional vitamin D nuclear receptor. *Proc Natl Acad Sci U S A*. 2004;101:1589–1594.
41. **Komori T.** Regulation of bone development and extracellular matrix protein genes by RUNX2. *Cell Tissue Res*. 2010;339:189–195.
42. **Takasu H, Sugita A, Uchiyama Y, Katagiri N, Okazaki M, Ogata E, Ikeda K.** c-Fos protein as a target of anti-osteoclastogenic action of vitamin D, and synthesis of new analogs. *J Clin Invest*. 2006;116:528–535.
43. **Matsuo K, Irie N.** Osteoclast-osteoblast communication. *Arch Biochem Biophys*. 2008;473:201–209.
44. **Raisz LG.** Pathogenesis of osteoporosis: concepts, conflicts, and prospects. *J Clin Invest*. 2005;115:3318–3325.
45. **Zhao C, Irie N, Takada Y, Shimoda K, Miyamoto T, Nishiwaki T, Suda T, Matsuo K.** Bidirectional ephrinB2-EphB4 signaling controls bone homeostasis. *Cell Metab*. 2006;4:111–121.
46. **Baldock PA, Thomas GP, Hodge JM, Baker SU, Dressel U, O'Loughlin PD, Nicholson GC, Briffa KH, Eisman JA, Gardiner EM.** Vitamin D action and regulation of bone remodeling: suppression of osteoclastogenesis by the mature osteoblast. *J Bone Miner Res*. 2006;21:1618–1626.
47. **Peppone LJ, Hebl S, Purnell JQ, Reid ME, Rosier RN, Mustian KM, Palesh OG, Huston AJ, Ling MN, Morrow GR.** The efficacy of calcitriol therapy in the management of bone loss and fractures: a qualitative review. *Osteoporos Int*. 2010;21:1133–1149.